# Quality by design based development, characterization, and optimization of a biohybrid collagen-silver nanoparticles with mupirocin

Rajandurai BABY ROSELIN [1] iD, Veintramuthu SANKAR[1]* iD, Muthiah RAMANATHAN[2] iD

[1] Department of Pharmaceutics, PSG College of Pharmacy, Coimbatore, India, 641 004.
Affiliated to TN Dr.M.G.R Medical University, Guindy, Chennai, India. 600 032.
[2] Department of Pharmacology, PSG College of Pharmacy, Coimbatore, India, 641 004.
*Corresponding Author. E-mail: sansunv@yahoo.co.in (V.S.); Tel.+91-984-229 07 01.

**ABSTRACT:** Wound healing is a complex process triggered by skin injury, and has increased attention on chronic wounds due to serious health problems and decline in life quality. The development of a biohybrid formulation using a synergistic technique involves a promising strategy for addressing various pathological manifestations of chronic wounds. This research aims to investigate the efficacy of beta-cyclodextrin (BCD) and sodium borohydride as a reducing agent in development of biohybrid collagen-based silver nanoparticles through a chemical reduction method with mupirocin (Col-AgNP-MUP). The Col-AgNP-MUP was developed and optimized to determine the best-reducing agent employing response surface methodology with critical quality attributes. The optimized formulation was characterized and demonstrated for its *in-vitro* cytotoxicity using a 3T3-L1 fibroblast cell line. The formulation, developed through chemical reduction method with BCD. The UV-vis spectroscopy exhibits a $\lambda_{max}$ at 402 nm and compatibility through Fourier transform Infrared spectroscopy (FTIR) studied. The particle size, polydispersity index (PDI), zeta potential(ZP) and entrapment efficiency(EE) were determined to be 188.4 nm, 0.176, 36.7 mV and 85.21 % respectively. The X-ray diffraction (XRD) indicates an amorphous peak owing to collagen matrix. Atomic force microscopy (AFM) and High-Resolution Transmission electron microscopy (HR-TEM) confirm a spherical shape of particles. *In-vitro* drug release studies showed efficacy at pH 7.4, suitable for the increased pH of chronic wounds. The *in-vitro* biocompatibility investigations demonstrated the Col-AgNP-MUP did not cause any toxicity. The study paves the work for developing a novel anti bacterial wound dressing.

**KEYWORDS**: Collagen; Mupirocin; Silver nanoparticles; Wound healing; QbD.

## 1. INTRODUCTION

Wound healing is a complex and dynamic mechanism triggered by the development of skin injury. An impairment of the integrity of the skin leads to the formation of wounds. A chronic wound is a skin injury impeded or delayed in healing through typical processes of wound healing stages. To expedite wound healing, it makes use of connective tissues, blood vessels, extracellular matrix (ECM) and several proinflammatory cytokines and growth factors[1].

Globally, the prevalence of chronic wounds is approximately 1.51 to 2.21 per 1000 people according to Martinengo et al[2].The chronic wound is frequently characterized by infection, formation of biofilm, inflammation, elevated metalloproteinase synthesis and decreased extracellular matrix (ECM), enhanced fibroblast senescence, and reduced collagen production[3]. Chronic wounds are primarily caused by bacterial infections which is due to the presence of gram-positive and gram-negative bacteria[4]. Therefore, the development of a formulation with the capability to treat microbial infections and accelerate wound healing requires a biomaterial-based treatment for synergistic activity.

The extracellular matrix (ECM) is an acellular part of the connective tissues essential for the healing of wounds. Collagen, elastin, fibronectin, laminin, tenascin, proteoglycans, glycosaminoglycan, and hyaluronan are the primary components of ECM and provide strength and cushioning to the cells of ECM[5]. Collagen makes up the majority of the proteins with 85 % of its dry weight, in the ECM of skin and tendons. It possesses distinctive and special characteristics, that are advantageous, like good biocompatibility, biodegradability, hydrophilicity, and low antigenicity[6]. It acts as an inherent substrate for cell adhesion, proliferation, and migration, concurrently augmenting the mechanical strength and elasticity during tissue repair. The natural characteristics and biomimetic properties of collagen make a growing

variety of collagen-based products in the field of regenerative medicine [7]. Currently, collagen-based drug delivery systems can be found in the fields of cosmetics, dental applications, tissue engineering, and wound healing products. It can be extracted from different types of animal tissue and marine sources have been combined with other active molecules for enhancement of wound healing rate.

Mupirocin, a pseudomonic acid antimicrobial agent, exhibits bacteriostatic effects at low concentrations and bactericidal effects at high concentrations against primary and secondary skin infections. Mupirocin has wide spectrum activities against gram-positive bacteria and is less active against gram-negative organisms [8]. Mupirocin is active against *Staphylococcus aureus* and *Streptococcus pyogenes.* The mechanism of action of mupirocin is, specifically, and reversibly binds to the enzyme isoleucyl transfer-RNA synthetase in bacteria, which inhibits the production of proteins in the bacteria. Mupirocin does not have cross-resistance with any other antibiotic because of its distinct mode of action[9]. Unfortunately with the wide use of mupirocin in practice gradually emerging drug resistance against organisms globally.

Nanomaterial-based wound healing has recently emerged as an important approach for promoting wound repair and inhibiting wound infections. Silver nanoparticles are attractive due to their increased surface area with smaller particle size and good interaction with the bacterial cell membrane leads silver nanoparticles to demonstrate enhanced antibacterial activity against gram negative microorganism[10]. Additionally, it is non-cytotoxic and quite effective at low concentrations. AgNPs enable antibiotics to work together, allowing them to penetrate the bacterial cell wall. They also have the ability to control pro-inflammatory cytokines at the site of a wound, promoting tissue regeneration and wound healing without causing scar tissue[11].

We used the Quality by Design (QbD) approach, which provides a distinctive chance to create a high-quality product. It originates with a known objective and investigates critical process parameters (CPP) and critical material attributes (CMA) to develop a final product with desired Critical Quality Attributes (CQAs). DoE is a software program that can be used for QbD purposes during the development of a formulation for understanding the main and interaction impacts of numerous CPPs [12]Dhasmash et al.Numerous investigations have been focused on developing of combination of antibiotics with nanotechnology for the development of wound dressing material with biopolymer. There is an evidence supporting the enhancement of antibiotics activity by acting synergistically with biopolymers in nanotechnology[13]. The Beta cyclodextrin has a role in improving the delivery, solubility and stability of therapeutic agents used in wound care[14].

The current study aimed to formulate a biohybrid collagen-based silver nanoparticle with mupirocin wound dressing materials, using the QbD approach, and to evaluate its cytotoxicity using 3T3- L1 fibroblasts cell line through *in- vitro* studies.

## 2. RESULTS AND DISCUSSION

### 2.1. Preparation and optimization of COL-AgNP-MUP

#### 2.1.1. QbD optimization and analysis of Results

The design of experiments was used to optimize the effect of factors on their response and allow prediction of process behavior within the design space. D-optimal designs are linear optimizations depending on a chosen optimality parameter and the model to be fitted. The set of combinations designated as the candidate set is where the D-Optimal approach chooses which possibilities to include in the design space. Stepping and swapping is a common method used by the computer program to choose a group of test runs. The D-optimal design is a desirable option when design space is limited [15,16].

Table 1, depicts the actual design factors as a process (X1-X2), material (X3), and categorical(X4) variables, and Table 2, shows the responses such as particle size(Y1), polydispersity index(Y2), zeta potential (Y3) and entrapment efficiency (Y4) was studied for the 24 experimental formulations. By applying mathematical equations and statistical measurement through experiment design, it analyses the effects of the independent variables (factors) on the dependent variables (responses) and provides the optimal formula. QbD is a critical step in the process and product variable optimization for generating the necessary CQAs of the formulation. To optimize the parameters and to achieve the best outcomes, the desirability approach was applied[15,17].

**Table 1.** Experimental Design for the optimization of AgNP-MUP formulation

| Formulation | X1 (min) | X2 (°C) | X3 (mM) | X4 (mM) |
|---|---|---|---|---|
| 1 | 20 | 80 | 3 | BCD |
| 2 | 33.8926 | 44.6 | 2.45829 | BCD |
| 3 | 55 | 58.1 | 5 | NaBH$_4$ |
| 4 | 60 | 80 | 1 | BCD |
| 5 | 60 | 80 | 5 | BCD |
| 6 | 20 | 43.4 | 3 | NaBH$_4$ |
| 7 | 60 | 20 | 1 | NaBH$_4$ |
| 8 | 20 | 80 | 5 | NaBH$_4$ |
| 9 | 20 | 20 | 5 | BCD |
| 10 | 20 | 80 | 1 | NaBH$_4$ |
| 11 | 20 | 20 | 5 | BCD |
| 12 | 60 | 80 | 3 | NaBH$_4$ |
| 13 | 20 | 43.4 | 3 | NaBH$_4$ |
| 14 | 40 | 50 | 5 | BCD |
| 15 | 54 | 40.7 | 1 | BCD |
| 16 | 20 | 20 | 1 | BCD |
| 17 | 36 | 20 | 3 | NaBH$_4$ |
| 18 | 60 | 20 | 3 | BCD |
| 19 | 44.8 | 64.1 | 1 | NaBH$_4$ |
| 20 | 20 | 20 | 1 | BCD |
| 21 | 60 | 20 | 1 | NaBH$_4$ |
| 22 | 60 | 20 | 5 | NaBH$_4$ |
| 23 | 45.2 | 77 | 3 | BCD |
| 24 | 20 | 80 | 5 | NaBH$_4$ |

### *2.1.2. Statistical optimization and evaluation of dependent variables*

ANOVA data will help to indicate which factors are statistically significant using variance. The high (coefficient of determination) value $R^2$ represents the better fit of the model for the particular response and the probability value $p<0.05$ represents a model is significant. The Adjusted $R^2$ values, in a regression model, take into consideration independent variables that do not show statistical significance. The discrepancy between the adjusted $R^2$ value and predicted $R^2$ values was less than 0.2. These findings demonstrated that the collected data are more statistically valid and fit the collected data quite well[18]. Figure 1, shows the plotting of 3D surface designs.

To study the interaction between factors and responses. The relative impact of the components can be ascertained by utilizing the coded equation to compare the factor coefficients. For every response, the generated data was converted into polynomial equations and represented as follows.

$Y1 = + 188.90 + 30.79C + 14.98D – 44.35AB + 30.73 AC – 19.76 BD -56.07 A^2$

$Y2 = + 0.4896 – 0.0607A + 0.1112B + 0.1496C – 0.0213D$

$Y3 = + 29.59 – 1.96A – 7.73C+3.16D -1.04AD - 4.19BC$

$Y4 = + 59.45 + 5.50A + 4.63B – 7.99C+ 4.81D – 6.80 AB +0.5937BC$

**Table 2.** Responses of AgNP-MUP formulation

| Formulation | Y1:PS(nm) | Y2 PDI | Y3: ZP(mV) | Y4: EE (%) |
|---|---|---|---|---|
| 1 | 201.2 ± 0.87 | 0.621 ± 0.01 | 31.9 ± 0.15 | 68.0 ± 0.30 |
| 2 | 120.4 ± 0.65 | 0.523 ± 0.02 | 29.3 ± 0.15 | 63.0 ± 0.41 |
| 3 | 187.4 ± 0.90 | 0.761 ± 0.02 | 15.0 ± 0.25 | 25 ± 0.26 |
| 4 | 67.8 ± 1.20 | 0.321 ± 0.03 | 40.1 ± 0.20 | 76 ± 0.15 |
| 5 | 105.6 ± 1.10 | 0.632 ± 0.04 | 18.2 ± 0.15 | 47 ± 0.20 |
| 6 | 80.4 ± 0.80 | 0.463 ± 0.02 | 20.1 ± 0.1 | 43 ± 0.15 |
| 7 | 38.6 ± 0.86 | 0.126 ± 0.01 | 35.4 ± 0.15 | 72 ± 0.20 |
| 8 | 178.6 ± 1.05 | 1 ± 0.03 | 21.1 ± 0.15 | 46 ± 0.20 |
| 9 | 116.6 ± 1.05 | 0.639 ± 0.01 | 40.3 ± 0.76 | 42 ± 0.30 |
| 10 | 196.5 ± 0.92 | 0.293 ± 0.02 | 45±1 | 69.2 ± 0.2 |
| 11 | 116.6 ± 1.20 | 0.358 ± 0.01 | 32.1 ± 0.23 | 39 ± 0.15 |
| 12 | 142 ± 0.75 | 0.508 ± 0.01 | 20.5 ± 0.2 | 58 ± 0.20 |
| 13 | 80.4 ± 0.83 | 0.632 ± 0.02 | 25 ± 0.26 | 45 ± 0.20 |
| 14 | 261.7 ± 0.90 | 0.231 ± 0.01 | 34 ± 0.26 | 61 ± 0.25 |
| 15 | 156.2 ±1.11 | 0.326 ± 0.02 | 40 ± 0.30 | 85 ± 0.2 |
| 16 | 88.3 ± 0.85 | 0.324 ± 0.01 | 45 ± 0.4 | 53 ± 0.26 |
| 17 | 191.3 ±1.20 | 0.251 ± 0.02 | 26.0 ± 0.35 | 43 ± 0.20 |
| 18 | 232.5 ± 0.95 | 0.463 ± 0.01 | 28.0 ± 0.32 | 68 ± 0.32 |
| 19 | 123 ± 0.62 | 0.462 ± 0.01 | 39.2 ± 0.1 | 65 ± 0.2 |
| 20 | 150.6 ± 1.05 | 0.423 ± 0.01 | 30 ± 0.25 | 64 ± 0.26 |
| 21 | 69.9 ± 0.36 | 0.12 ± 0.03 | 32 ± 0.26 | 63 ± 0.15 |
| 22 | 223 ± 0.52 | 0.561± 0.02 | 18.0 ± 0.25 | 58 ± 0.1 |
| 23 | 174.6 ±1.25 | 0.623 ± 0.01 | 29.0 ± 0.25 | 67 ± 0.17 |
| 24 | 178.3 ±1.21 | 1 ± 0.1 | 13.0 ± 0.20 | 55 ± 0.36 |
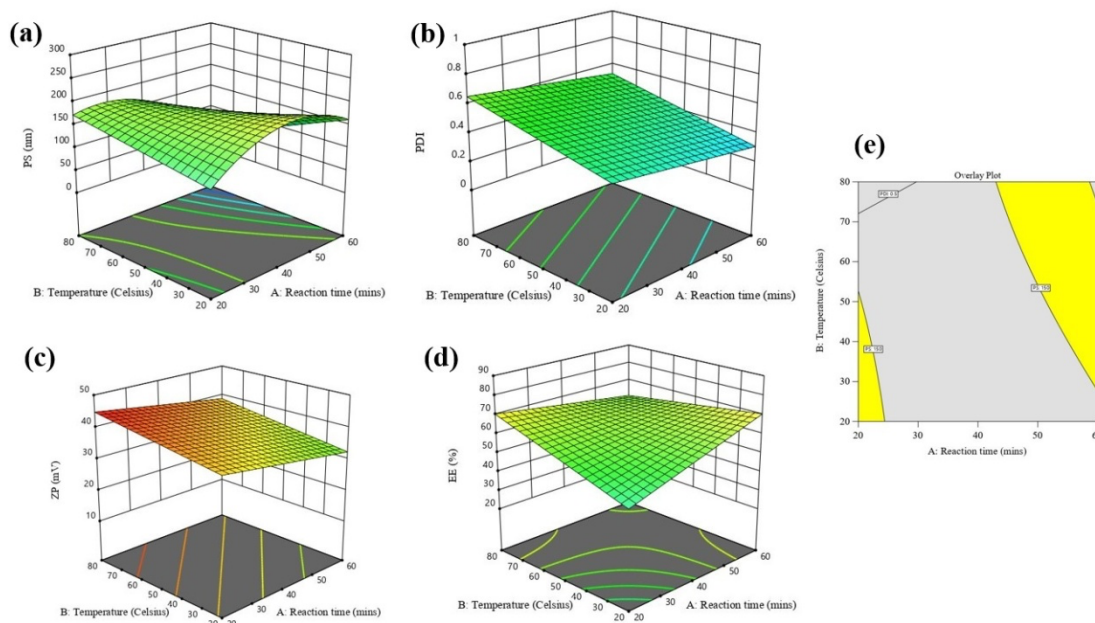


**Figure 1.** 3D response surface plots showing the influence of CMA and CPP on CQA,
a) Particle size b) Poly Dispersity Index c) Zeta Potential d) Encapsulation efficiency e) Overlayplot

***2.1.3.*** *Impact of independent variables on particle size*

Table 2, shows the PS range between 38 nm to 261nm. The analysis was done on the effects of factors X1 to X3 on the formulation PS. An increase in $AgNO_3$ concentration (X3) significantly increases the particle size. Similarly, BCD also shows a positive effect on particle size. The PS was significantly ($p<0.05$) affected by silver nitrate concentration. Increased particle size may be due to particle aggregation and precipitation of the nanoparticle. Furthermore, an increase in reaction time and temperature decreases the particle size. This may be explained due to the larger surface area[19].

Table 3, 4 display ANOVA data with an adequate precision value. If the signal-to-noise ratio is measured, a result greater than 4 indicates that the model has acceptable discrimination. In this model, the adequate precision value is 10.9729. The reduced quadratic model was fitted for the mean particle size with the $R^2$ value 0.7249. In the diagnostics, the normal plot of residuals follows under the straight line which is normal distribution data shown in Figure 2a, b. This data shows the variables that are not included as a factor or response in the analysis but can affect the interpretation between variables. It also shows a random scatter. Figure 2.c indicates the $\lambda_{max}$ value is 1 based upon the curve produced by the natural log of the sum of squares of the residuals.
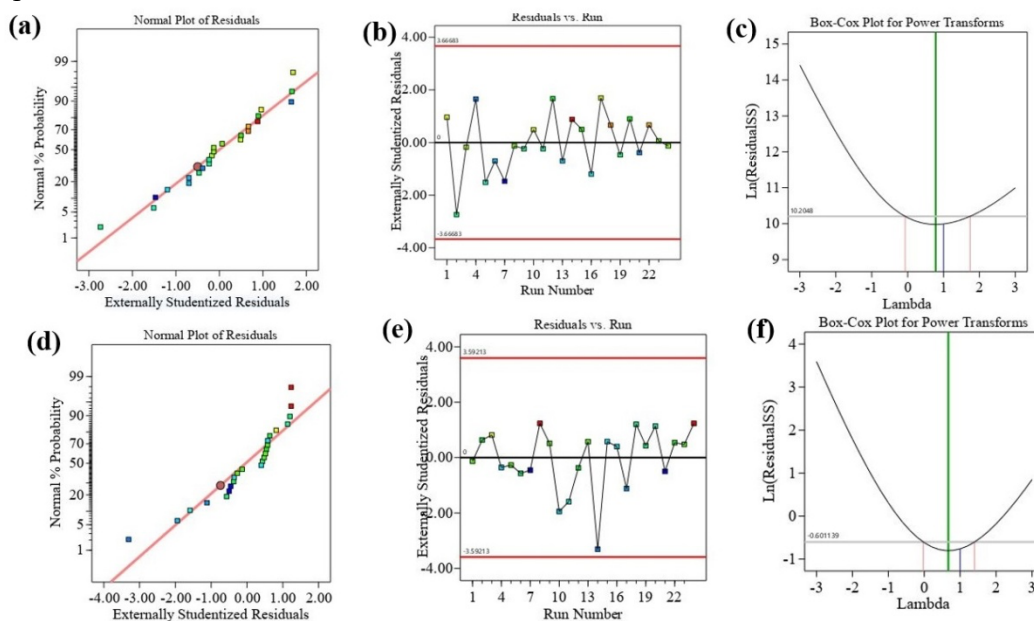


**Figure 2.** Particle size a) Normal plot of residuals b) Residuals vs Run c) Box-Cox plot
Zeta potential d) Normal plot of residuals b) Residuals vs Run c) Box-Cox plot

**Table 3.** Model statistics data of the optimal design of formulations

| Responses | Model | R² | Adjusted R² | Predicted R² | Adequate Precision |
|---|---|---|---|---|---|
| **PS (nm)** | Reduced Quadratic model | 0.7249 | 0.6279 | 0.4417 | 10.9729 |
| **PDI** | 2FI model | 0.8559 | 0.5426 | 0.4029 | 8.9813 |
| **ZP(mV)** | Reduced 2FI model | 0.7134 | 0.6338 | 0.4744 | 9.2821 |
| **EE (%)** | Reduced 2FI model | 0.8036 | 0.7177 | 0.5207 | 9.1099 |

***2.1.4.*** *Impact of independent variables on PDI*

Table 3 depicts the PDI range between 0.2 to 1. The temperature(X2) and concentration of silver nitrate (X3) have a significant impact on the PDI. Increases in X2 and X3 variables increase the PDI. These PDI values are highly polydisperse due to the collagen matrix having a tendency to form aggregates. The PDI of the formulation is significantly ($p<0.05$) affected by temperature and silver nitrate concentration [13]. It might affect the stability of the formulation. The smaller the PDI the more homogenous nanoparticles produced[20]. BCD does not have any significant effect on the PDI. But if reaction time increases there may be a chance for the excellent PDI value for the formulation. The 2FI model was fitted for the mean PDI with the $R^2$ value of 0.8559. Figure 2 d, e, f shows the normal plot, Residual vs run, and Box-cox plot respectively.

The plot displays the maximum power of the transformation through the representation of $\lambda_{max}$. It shows the $\lambda_{max}$ 1 with random scatter, suggesting that no transormation required.

**Table 4.** ANOVA results for the optimal design of formulations

| Responses | Source | Sum of Square | Degrees of freedom | Mean Square | F-Value | P-Value | Status |
|---|---|---|---|---|---|---|---|
| **PS (nm)** | Model | 57597.62 | 6 | 9599.60 | 7.47 | <0.0005 | Significant |
| | Residual | 21854.22 | 17 | 1285.54 | | | |
| | Lack of fit | 19451.72 | 12 | 1620.98 | 3.37 | 0.0943 | not significant |
| | Pure error | 2402.50 | 5 | 480.50 | | | |
| **PDI** | Model | 0.7693 | 4 | 0.1923 | 7.82 | <0.0007 | Significant |
| | Residual | 0.4673 | 19 | 0.0246 | | | |
| | Lack of fit | 0.4086 | 14 | 0.0292 | 2.49 | 0.1606 | not significant |
| | Pure error | 0.0587 | 5 | 0.0117 | | | |
| **ZP(mV)** | Model | 1431.31 | 5 | 286.26 | 8.96 | <0.0002 | Significant |
| | Residual | 574.97 | 18 | 31.94 | | | |
| | Lack of fit | 380.67 | 13 | 29.28 | 0.7536 | 0.6872 | not significant |
| | Pure error | 194.29 | 5 | 38.86 | | | |
| **EE (%)** | Model | 2700.91 | 7 | 385.84 | 9.35 | <0.0001 | Significant |
| | Residual | 660.11 | 16 | 41.26 | | | |
| | Lack of fit | 512.11 | 11 | 46.56 | 1.57 | 0.3227 | not significant |
| | Pure error | 148.00 | 5 | 29.60 | | | |

### *2.1.5. Impact of independent variables on zeta potential*

For antibacterial property of wound dressings, the presence of positive zeta potential facilitates the interaction between the particles and microorganism surface [13]. Table 3 shows the ZP range between +13 to +45 mV. The influence of the X1 to X4 shows the negative zeta potential. However, the positive zeta potential effect is attributed to the presence of collagen and its isoelectric pH.

Collagen shows more solubility in acidic pH and the zeta potential value is increased to attain more stability. A reduced 2FI model was fitted for the mean ZP with the $R^2$ value of 0.7134. Figure 3 a, b, c shows the plotted graph which indicates the normal distribution data and $\lambda_{max}$value 1 with the random scattering effect.

### *2.1.6. Effect of Independent Variables on Entrapment Efficiency*

The EE of the formulation shows the ZP range varies from 25% to 85 % in Table 3. The Reduced 2FI model was fitted for the mean EE(%) with the $R^2$ value of 0.8036. X3 shows a significant (p<0.0001) effect on the formulation. It indicates that when silver nanoparticles are present in the collagen matrix, there is a larger chance of drug entrapment. As, Nanoparticles develop and stabilize, they attach to the functional groups on the polymer[21]. Figure 3 d, e, f represents the normal distribution data with $\lambda_{max}$value 1 and with random scattering.

### *2.1.7. Optimization and Validation of Results*

The factor values can be set by the analyst using point prediction. The interval estimations and projections are generated by the models. Confirmation measures the model's prediction interval against the average of a subsequent sample. The model is verified if the sample average falls within the expected range. Usually, confirmation is carried out at or close to the factor settings that numerical optimization suggests. PS and EE are most significantly impacted by the type of reducing agent (BCD) (p<0.05). Based on the statistical analysis, Beta cyclodextrin shows a successful reducing agent valuable for increasing stability, and drug

release while retaining safety and efficacy in the formation of Col-AgNP-MUP useful for further development of ointment for the treatment of wound healing.

A point that maximizes the desirability function is studied by numerical optimization. If the goals were easily attained and better outcomes were expected, through the attractiveness desirability of 1. The predicted values for PS, PDI, ZP, and %EE of Col-AgNP-MUP are shown in table 5. The predicted value is 160.1 nm, 0.352,40.0 mV and the experimentally optimized value is 188.4 nm, 0.176, 36.7 mV, and 85.21 % respectively. The graphical optimization represents the overlay plot for the responses in Figure 1 e.
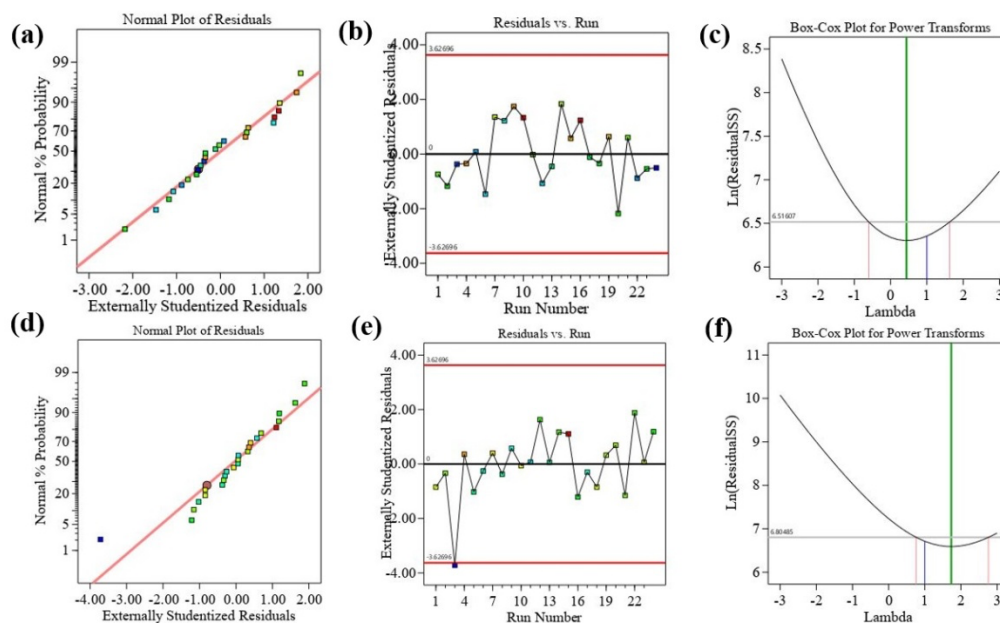


**Figure 3.** PDI a) Normal plot of residuals b) Residuals vs Run c) Box-Cox plot,
Entrapment efficiencyd) Normal plot of residuals e) Residuals vs Run f) Box-Cox plot

**Table 5.** Predicted and observed responses of the optimal formulation prepared using BCD as a reducing agent.

| Variables | Optimized values | Responses | Predicted Values | Observed Values |
|---|---|---|---|---|
| X1( min) | 44.213 | Y1 (PS) | 160.172 | 188.4 ± 10 |
| X2(°C) | 58.161 | Y2 (PDI) | 0.352 | 0.176 ± 0.01 |
| X3(mM) | 1.21 | Y3 (ZP) | 40.042 | 36.7 ± 1.27 |
| X4(reducing agent type) | BCD | Y4 (EE) | 75.238 | 85.21 ± 2.25 |

## 2.2. Characterization of the Optimized COL-AgNP-MUP dispersions

### 2.2.1. UV-visible spectroscopy

The localized surface Plasmon resonance (SPR) of the synthesized metallic nanoparticles is examined using UV-Vis spectroscopy. Figure 4a shows the formation of the Col-AgNP-MUP by the indication of color change from colorless to yellow color. Figure 4b depicts the plasmonic absorption peak observed around 402 nm. The appearance of an absorption peak found at a 400-450 nm wavelength is an indication of smaller size silver nanoparticle formation[22]. They interact strongly with light because light at certain wavelengths excites the conduction electrons on the metal surface, causing an oscillation collectively that results in high-surface Plasmon resonance.This interaction gives useful information about the size, shape and size distribution of the particles and the sharpness of the UV-Vis peak reflects the monodispersity of the particles. The absorption peak of this current data agrees with data reported by amutha et al and Subha et al.[23,24].
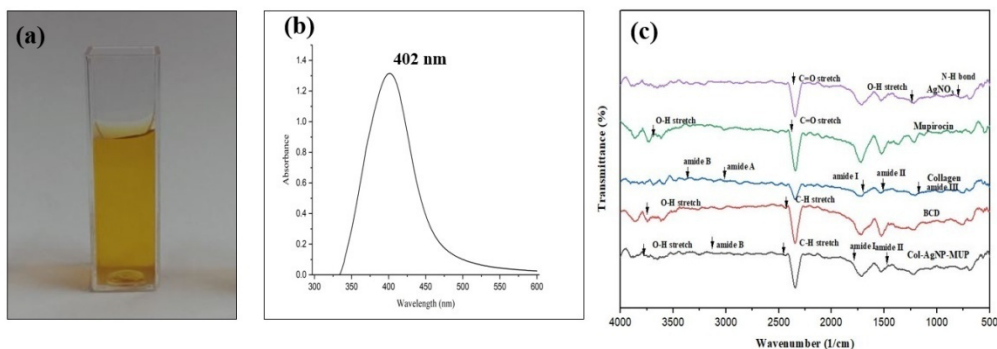
**Figure 4.** a) Col-AgNP-MUP dispersion b) UV-Vis spectra c) FTIR spectra

*2.2.2. FT-IR spectra*

The chemical and physical properties of the optimized Col-AgNP-MP were examined through the FT-IR spectra. Figure 4.c. Illustrates the functional group of the silver nitrate, Mupirocin, Collagen, BCD, Col-AgNP-MUP. The FT-IR spectra of the pure $AgNO_3$ exhibit an absorption peak at 3232 cm$^{-1}$ and it is responsible for the O-H stretching vibration. 1374 cm$^{-1}$ and 1127 cm$^{-1}$ peak indicates the presence of O-H bending. 825 cm$^{-1}$ indicates the N-H rocking bond between nitrogen and hydrogen. Mupirocin shows the FT-IR spectra region at 3676 cm$^{-1}$ represented to the medium sharp O-H stretching and 3101 cm$^{-1}$ respect to weak O-H stretching, at 1726cm$^{-1}$ is associated to the C=O stretching, 1648 cm$^{-1}$ peak is caused by conjugated C=O stretching, 1229cm$^{-1}$peak obtained due to the presence of ester acetate C-O stretching, and 1147cm$^{-1}$ exhibits the C-O-C stretching[23].

Collagen exhibits an absorption peak at 1683 cm$^{-1}$ for amide I with C=O stretching, 1525 cm$^{-1}$ for amide II with N-H bend-linked stretching, and 1240 cm$^{-1}$for amide III $CH_2$ group stretching. The N-H stretch involved in the hydrogen bond is exhibited by amide A at a peak of 3150 cm$^{-1}$, whereas the $CH_2$ asymmetric stretching vibrations are represented by amide B at a peak of 2920 cm$^{-1}$[26]. BCD exhibits the region at 3736 cm$^{-1}$ associatedwith the O-H stretching vibration, and 1718 cm$^{-1}$ absorption associated with the C=O stretching group. 2341 cm$^{-1}$ exhibits C-H bond stretching vibrations. 1531 cm$^{-1}$ and 1377 cm$^{-1}$ peaks were attributed to the $CH_2$ bending vibration and C-O stretching vibration. C-O-C stretching vibration of BCD at 1128 cm$^{-1}$. The pyranose ring structure is visible at the peaks at 675 cm$^{-1}$and 545 cm$^{-1}$[27]. AgNP-MP coated collagen(AgNP-MP-Col) exhibits the entire major peak corresponding to the Mupirocin, Collagen, and AgNP, which is indicative of the absence of strong interactions between them. These results were also comparable with previous data, budhiraja. M et al.[28]

*2.2.3. Particle size, Zeta potential and Polydispersity index*

The measurement of nanoparticle size is commonly accomplished through using the technique of Dynamic Light Scattering (DLS). It provides the population of particles in a short duration.The optimized formulation is subjected to analyze its micromeritics property.The PS of the formulation was observed at 188.4 nm with the PDI value 0.176 which indicates highly monodispersed shown in Figure 5. Monodispersity and spherical shape of the formulation are also reflected by the sharpness of the DLS peak.

The zeta potential provides short and long term stability of the nanoparticles. The primary factor influencing the stability of nanoparticles is the repulsive force between charged molecules. The tendency of particles with charged surfaces near neutral zeta potential is to aggregate more quickly. The higher positive or negative charges ensure better stability. The optimized formulation was found to be +36.7 mV. It suggests that silver nanoparticles with mupirocin collagen complex reduced aggregation[26]. The particle size and zeta potential of the collagen-based formulations were observed to exhibit greater stability compared to the silver nanoparticles synthesized using other reducing agents as reported by the study conduted by prem santhi et al.[30]
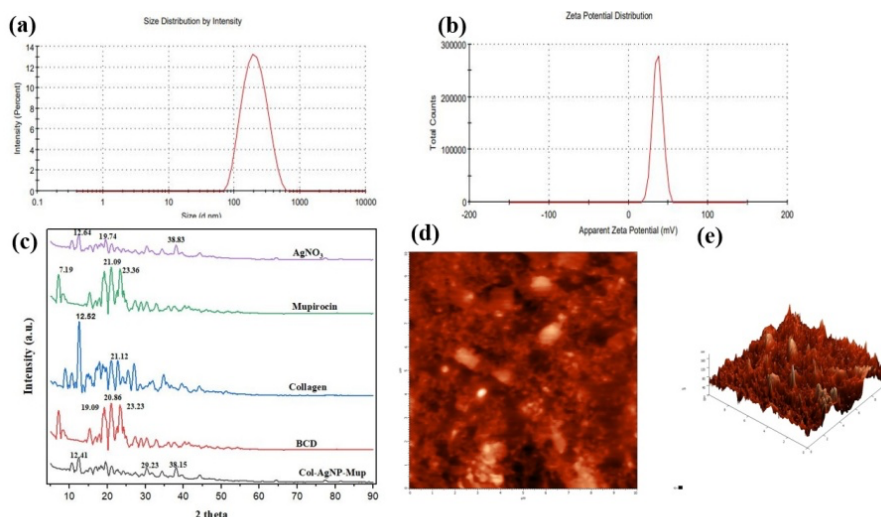
**Figure 5.** Optimized formulation a)particle size b) Zeta potential c) XRD spectra d) AFM 2D topography e) AFM 3D topography

2.2.4. Estimation of Entrapment Efficiency (EE %)

The EE % was represented as the proportion of the drug successfully entrapped within the collagen matrix. In the optimized formulation mupirocin exhibits an EE (%) of $85.21 \pm 2.25$ %. The EE (%) was observed to increase with silver nanoparticle- mupirocin interaction with increasing reaction time. F4, F7 and F15 show the entrapment efficiency ranging from $72 \pm 0.20$% to $85 \pm 0.2$%. F3 formulation has very low EE. This may be attributed to the increased silver nitrate concentration leads to increased particle size with previous data. [27].

*2.2.5. X-ray diffraction analysis*

The crystalline parameters and structural alterations of formulations are examined using the XRD instrument. The XRD spectra of silver nitrate, Mupirocin, Collagen, BCD, and Col-AgNP-MUP are shown in **Figure 5c.** Silver nitrate shows peaks at various $2\theta$ positions $12.64°$, $19.74°$, and $38.83°$ indicating the crystallinity nature. Mupirocin exhibited strong intense peaks at $7.19°$, $21.09°$ and $23.36°$ indicating the crystallinity of the drug. The collagen peak located at $12.52°$ and $21.12°$ indicates a slightly amorphous nature. The formulation exhibits a broad peak around $12.41°$, $29.23°$, and $38.15°$ indicating the amorphous nature attributed due to the collagen. The important crystalline peak is diminished due to the incorporation of AgNP-MUP in collagen for the optimized formulation [28].

*2.2.6. AFM analysis*

Surface topography, size, shape, and size distribution are all analyzed with nanoscale resolution by AFM analysis. Figure 5d,e shows the 2D and 3D topographical images of Col-AgNP-MUP with smooth surface morphology owing to the existence of Collagen capped AgNP-MUP. The average particle size is around 155 nm and it shows average surface roughness in 15.97 nm with monodipersed and spherical shape. The Root mean square(Sq) is a dispersion parameter to characterize the surface roughness and it shows around 21.13 nm. The skewness ($S_{sk}$)is used to measure the data distribution and the results showed the distribution is moderately skewed.The kurtosis($S_{ku}$) is a measure of the tailedness of the frequency distribution value owing to the sharpness of the peak. The results showed the platykurtic (<3) type of kurtosis for the formulation.The current findings align with observations made through HR-TEM. Similarly , the literature results have elucidated that the spherical morphology of the particles is attributed to the presence of reducing agent according toVenkata S. et al[33].

*2.2.7. HR-TEM–EDS analysis*

The morphology of the optimized nanoformulation was observed in HR-TEM. It showed smooth spherical shape particles and the average diameter of the particle size is $152 \pm 1.27$nm with no signs of aggregation illustrated in Figure 6a,b. According to some researcher's reports, the smaller size is the effective size for nanoparticles against bacteria, since the higher surface area of the particles can assist in interacting

with the bacterial membranes[29]. Figure 6c demonstrates the spots within the SAED pattern that can reveal the face-centered cubic (FCC) structure is crystalline nature.

The EDS spectra is an analytical technique mainly used for the identification of different elemental compositions in a sample. It can also estimate the concentration of specific elements and the spectra of the optimized formulation. The Figure 6d shows the strong signal peakof the presence of Agin the L series with a weight percentage of 50%, which describes the purity of the silver. In addition, some weak peaks are also present due to carbon, oxygen, nitrogen and hydrogen[30].
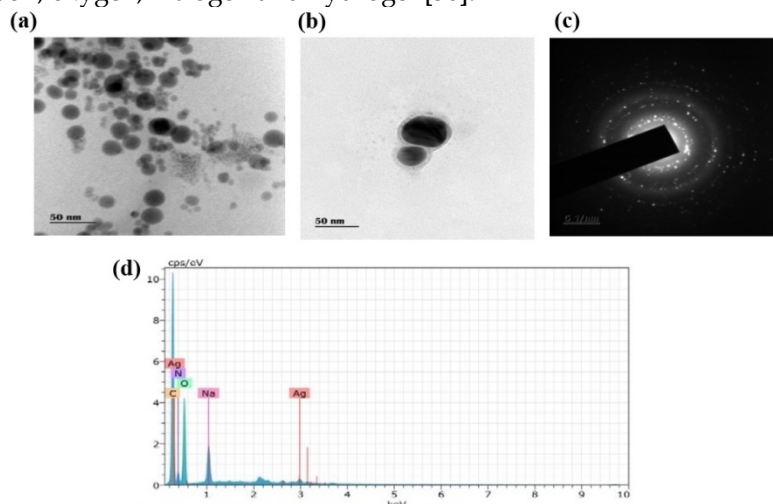


**Figure 6.** Optimized formulation (a, b) TEM micrographs  c) SAED pattern d) EDX spectra

*2.2.8. In-vitro drug Release*

Wounds require effective drug release due to their varying pH levels. The *in-vitro* release profiles of MP from the optimal formulation were analyzed with three different buffered pH solutions. Three distinct buffered pH solutions were used to analyze the MP *in-vitro* release profiles from the optimal formulation. The pH 5.5(the normal skin), pH range 6.8 to pH 7.4 which corresponds to the acute to chronic wound. The *in-vitro drug* release observed remarkable differences in the rate and amount of MP release from the formulation based on pH displayed in Figure.7.a. A maximum drug release was found to be 82.6 ± 2.08 % after 48 h from AgNP-MUP-loaded collagen at pH 7.4. This might be attributed due to the smaller particle size with AgNP using beta-cyclodextrin (hydrophilic in nature)as a reducing agent. In this case, alkaline also has an influence in increased drug release through the diffusion mechanism. Furthermore, a decrease in pH to 6.8 showed decreased drug release such as 71.6 ± 3.22 %. In contrast**,** at pH 5.5 shows the lowest release of 59.63 ± 1.20% at 48 h. To control the risk of infection on the wound requires rapid release of drugs from the collagen matrix[36].

**Table 6.** Optimized formulation release kinetic mechanism in different pH

| pH | Zero order | | First order | | Higuchi | | Korsemeyer-peppas | | Hixon-Crowell | |
|---|---|---|---|---|---|---|---|---|---|---|
| | $r^2$ | $k_0$ | $r^2$ | $k_1$ | $r^2$ | $k_H$ | $r^2$ | N | $r^2$ | $k_{HC}$ |
| **5.5** | 0.7178 | 1.565 | 0.9117 | 0.026 | 0.9739 | 8.588 | **0.9713** | 0.557 | 0.8629 | 0.008 |
| **6.8** | 0.5520 | 2.146 | 0.9377 | 0.052 | 0.9707 | 12.148 | **0.9712** | 0.489 | 0.8818 | 0.015 |
| **7.4** | 0.4824 | 2.392 | 0.9565 | 0.066 | 0.9728 | 13.659 | **0.9863** | 0.466 | 0.9158 | 0.019 |

The optimized formulation release data was kinetically analyzed through linear regression analysis using the zero-order, first-order, Higuchi, Korsemeyer-Peppas, and Hixson-Crowell models. Korsemeyer-Peppas indicates the goodness of fit using $r^2$ value, and the release exponent exhibits Non fickian release based upon the n values found to be 0.557,0.489 and 0.466 with respect to the pH 5.5, 6.8 and 7.4 respectively shown in Table 6[32].
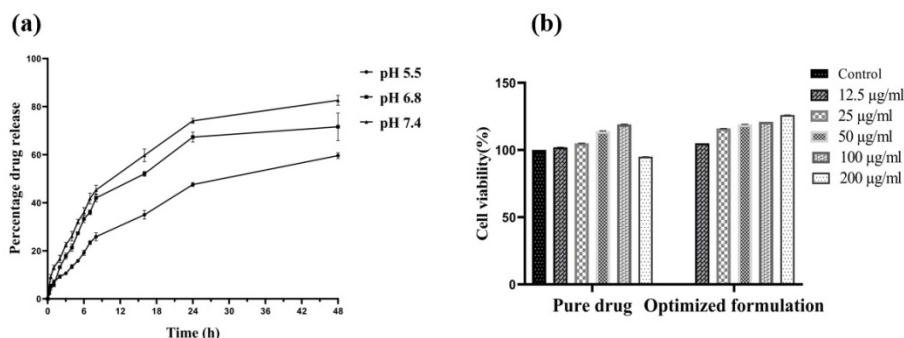
**Figure 7.**a) *In-vitro* drug release profiles of optimized formulation at different pH. b) *In-vitro* cell viability.

*2.2.9. In-vitro cytotoxicity*

The cell growth and adhesion indicate the biocompatibility of the sample and it is also typically involved in assessing the potential toxic effects of formulation on cells involved in wound healing applications. The 3T3 –L1 fibroblasts cell line exposure after 24 hr of the optimized formulation resulted absence of cell death(> 90% cell viability) up to 200 µg/ml concentration compared with the control group as shown in Figure 7b [38]. The pure MP showed decreased viability in the same concentration. The viability of fibroblast cells remains above 90% across all the concentration after 24 hr. This observation indicates that the optimized formulation does not induce any significant ($p<0.05$) difference in cytotoxic effect on fibroblasts. This outcome can be attributed to the biologically derived or inherently non-toxic nature of the individual constituents within our formulation. For the first time, no cytotoxic dose concentrations were documented.

## 2.3. Storage stability assessment

**Table 7.** Stability studies

| Assesment condition | Temperature/RH (°C) | Particle size (nm) | PDI | ZP (mV) | EE (%) | Physical appearance |
|---|---|---|---|---|---|---|
| 0 day | | 188.4±0.1 | 0.176±0.01 | 36.7±0.1 | 85.21±0.2 | Dark yellow color |
| 1st month | 04±0.5 °C/no RH | 180.5 ± 0.65 | 0.182±0.02 | 38.6±0.3 | 84.26±0.1 | Dark yellow color |
| | 25±0.2 °C/60 ± 5% | 170.9± 0.26 | 0.176±0.03 | 37.6±0.2 | 72.12 ± 0.15 | Dark yellow color |
| | 30± 2 °C/65 ± 5 % | 264.0±0.45 | 0.545±0.01 | 30.2±0.2 | 65.16 ± 0.04 | Pale yellow color |
| 3rd month | 04±0.5 °C/no RH | 170.9±0.17 | 0.062±0.02 | 39.7±0.1 | 72.14± 0.05 | Pale yellow color |
| | 25±0.2 °C/60 ± 5% | 132.1±0.26 | 0.161±0.01 | 26.5±0.1 | 65.43± 0.04 | Pale yellow color |
| | 30± 2 °C/65 ± 5 % | 208.6 ± 0.4 | 0.302±0.02 | 21.3±0.2 | 55.21± 0.05 | Clear white color |
| 6th month | 04±0.5 °C/no RH | 169.3±0.20 | 0.095±0.03 | 35.8±0.5 | 65.26± 0.15 | pale yellow color |
| | 25±0.2 °C/60 ± 5% | 105.6±0.15 | 0.210±0.01 | 29.3±0.2 | 48.86± 0.32 | Clear white color |
| | 30± 2 °C/65 ± 5 % | 155.3±0.2 | 0.274±0.02 | 21.4±0.1 | 28.45± 0.05 | Clear white color |

The stability studies data of the optimized formulation was shown in Table 7. The formulation had a dark yellow physical appearance when it was first noticed. After 1 month, the color changed into pale yellow, in the 3rd month further changed into a colorless solution and the nanoparticle get settled, the aggregation began at the end of both the first and third month at 30± 2 °C/65 % RH. The particle size and PDI value are increased, zeta potential and EE is also decreased in the first month. Furthermore, the formulation exhibited a notable reduction in entrapment efficiency (28.45%) at the end of the sixth month at a temperature of 30± 2 °C. Additionally, variations in zeta potential were observed after six month due to particle aggregation. However, all test-conditioned data revealed significant ($p<0.05$) variations in PS, ZP, and EE over six months. For a maximum of three months, this stability investigation found that 04±0.5 °C with no relative humidity and 25±0.2 °C/60% were the ideal storage conditions for the optimized formulations. The temperature exerts a significant influence on the diminution of stability. the poly dispersion of the particles get increased as per, Nisar ahmed et al, [39].

## 3. CONCLUSION

Through this study, QbD approach highlights that beta-cyclodextrin as a highly promising reducing agent for the development of biohybrid collagen-stabilized silver nanoparticles with mupirocin. The results of UV-visible and FTIR studies revealed the formulation compatibility. The morphological results of AFM and HRTEM revealed uniform size and shape in the formulation. The increased EE% and *in-vitro* drug release will release effective drug concentration for combating wound infections during surgical dressing application. The *in-vitro* cytotoxicity study demonstrated biocompatibility and enhanced proliferation and migration properties of fibroblasts at the wound site. Owing to its properties, it holds the potential for the development of collagen-based silver nanoparticles with antibiotic wound dressing tailored to address infections in wounds in the future.

## 4. MATERIALS AND METHODS

Mupirocin (MUP) is a topical antibiotic, which is generously gifted from fourrts India laboratories pvtltd, chennai. Type I collagen from bovine hide source (Previously extracted and characterized ), Silver nitrate ($AgNO_3$), Poly vinyl pyrrolidone (PVP), Glutaraldehyde were purchased from Himedia, Mumbai. Moly chem (Mumbai) supplied Beta-cyclodextrin (β-CD) Sodium hydroxide (NaOH) was obtained from Fisher Scientific, USA. Mouse embryonic fibroblasts (NIH 3T3-L1, Passage number 29) cell line was procured from the National Centre for cell science (NCCS), Pune for an *in-vitro* experimental study. 3-[4,5-dimethylthiazol-2-yl]-2,5 diphenyl tetrazolium bromide (MTT) purchased from Himedia, Mumbai. Dulbecco modified Eagle Medium (DMEM) was purchased from Gibco, Thermo Fischer, USA. All the chemicals and solvents utilized were analytical grade throughout the study.

### 4.1. Methodology

The QbD approach involves the statistical design of an experiment (DoE) for systematically optimize a formulation. Critical material attributes (CMAs) and critical processing parameters (CPPs) that affect the critical quality attributes (CQAs) of the final product are better understood with the use of QBD[40]. In the present study, Col-AgNP-MUP formulation optimization was performed by design expert software using D-optimal response surface design. (version 13.0, Stat Ease Inc., Minneapolis, USA). In order to examine the effects of these variables on the selected CQAs three numerical factors -such as reaction time(X1), reaction temperature(X2), the concentration of silver nitrate(X3), and one categorical factor (Reducing agent type-X4) were identified as CMAs and CPPs (Independent variables). The low and high levels of factors are shown in Table 8.

For response (dependent variables), the CQAs of formulations were particle size (PS, Y1), polydispersity index (PDI, Y2), zeta potential (ZP, Y3), and entrapment efficiency (EE, Y4) were characterized. The software yielded 24 runs and executed in triplicates (n=3). AgNP-MP formulations have been optimized for 4 responses with the objective being to achieve minimized PS, minimize PDI, and maximize ZP and EE(%). The highest multiple response method describes the desirability function with the highest value (ranges from 0 to 1) is chosen[35]. The optimal Col-AgNP-MP formulation was then prepared using the optimized independent variables. Each result was statistically analyzed and validated using analysis of variance (ANOVA).

### 4.2. Selection of the optimized formulation

The optimization of multiple responses using numerical and graphical analysis was done using the desirability function approach. The desirability function assigns a score between 0 and 1 for each response. Using numerical analysis, the individual desirability is subsequently combined to produce an overall desirability number. The ideal optimal formulation corresponds to a value close to 1. Followed by an optimized formulation was prepared and further characterized [36].

**Table 8.** Independent variables and dependent variables

| | Numerical factor (discrete) | Low level | High Level |
|---|---|---|---|
| X1 | Reaction time (min) | 20 | 60 |
| X2 | Temperature (°C) | 20 | 80 |
| X3 | **Numerical factor (Continuous)** | 1 | 5 |
| | AgNO$_3$ Concn (mM) | | |
| X4 | **Categorical factor** | **Applied Levels** | |
| | Reducing agent type | NaBH$_4$ | BCD |
| | **Responses** | **Optimization Goal** | |
| Y1 | PS | Minimize | |
| Y2 | PDI | Lowest | |
| Y3 | ZP | Highest | |
| Y4 | EE | Maximum | |

### 4.2.1. Preparation of Col-AgNP-MUP

The optimized formulation was synthesized by a bottom-up technique. Bovine type –I collagen previously extracted according to the procedure[43], was dissolved in 5 ml of acetic acid using 0.05 M concentration to form a collagen solution and was kept at 4° C for the following procedure. 1.5 mM BCD was added into 30 ml distilled water, and the mixture was stirred at a speed of 400 rpm. To this 10 ml of 25 mM NaOH solution was added slowly.

To the aforementioned beta-cyclodextrin based solution from DoE, the 1.9 mM AgNO$_3$ solution was gradually added for reaction at an optimized time and temperature. After the reaction, the solution color changed from colorless to dark yellow color. To this 100 mg of mupirocin was added and continuously stirred for 1 hr[44]. Finally, the silver nanoparticle with mupirocin was synthesized. To the 5 ml collagen solution, the above synthesized AgNP-MUP was gradually added with continuous stirring at 200 rpm for homogenized collagen coating. The procedure was carried out at 4° C.

### 4.2.2. Freeze-drying of Col-AgNP-MUP

The optimized Col-AgNP-MUP formulation was mixed with 0.5% polyvinyl pyrollidone as a cryoprotectant, and the homogenized formulation was kept using a freezer at -80° C overnight (Thermo Scientific freezer, USA). The frozen collagen-based nanoformulation was then lyophilized in a freeze drier (Lyodel, India) at -70 °C with 10$^{-3}$ mbar for 4 days to get dried powder. The yield was then stored in a tarsun tube for further analysis.

## 4.3. Characterization of the Optimized Col-AgNP-MUP

### 4.3.1. UV-Visible (UV-Vis) spectroscopy analysis

The synthesized biohybrid Col-AgNP-MUP was characterized by using UV-vis spectroscopy (UV-1601 PC Shimadzu, Japan)with a 1 cm path length cuvette. The absorption spectra ($\lambda_{max}$) of the sample were measured at the wavelength ranging between 300 to 600 nm[28].

### 4.3.2. Fourier transform infrared spectroscopy (FT-IR spectroscopy)

The Col-AgNP-MUP formulation FT-IR spectra were analyzed using FT-IR spectroscopy (FT-IR 8400S Shimadzu, Japan) to monitor the functional group changes after AgNP-MP. To create pellet, 2 mg of the freeze-dried formulation was combined with KBr. The pellets were then analyzed using 15 scans from 4000-400 cm$^{-1}$[28].

### 4.3.3. Particle size, polydispersity index and zeta potential analysis

The synthesized formulation was analyzed for its micromeritics property. The mean diameter of particles, PDI, and ZP of Col-AgNP-MUP was measured by Nano ZS 90 Zetasizer (Malvern, United Kingdom). PDI represents size distribution of formulation and surface charge represents as ZP of the optimized formulation according to Andrade P et al[38].

### 4.3.4. Entrapment Efficiency (EE%) analysis

The percentage of drug encapsulated inside the collagen matrix in relation to the total quantity of drug added is the investigation of entrapment efficiency. The ultracentrifugation method was utilised to ascertain it. The Col-AgNP-MP formulation was centrifuged for 30 minutes at 4°C at a speed of 12,000 rpm. The amount of unentrapped (free) drug in the supernatant solution was measured using UV-Visible spectroscopy (UV-1601 Shimadzu spectrophotometers, Japan) with proper dilution at a wavelength of 222 nm[46]. Finally based on the absorbance value the percentage(%) EE of Collagen-based formulation was calculated using equation: **1.**

EE(%) = (total amount of drug- Amount of unentrapped drug) / total amount of drug ×100

### 4.3.5. X-Ray diffraction spectroscopy (XRD)

X-ray diffraction pattern of the dried sample mupirocin, AgNP, collagen and Col-AgNP-MUP formulation was analyzed using X-ray Diffractometer (Empyrean, Malvern Panalytical) based on the Bragg-Brentano high definition high intensity principle. The operation involved applying a voltage of 40 kV with a step scanning of 0.02° and employing Cu Kα radiation (λ= 1.54 Å) and the scanning occurred within the 2θ range from 10° to 90° speed with 10° /min and a current of 30 mA according to srivatsan et al[47].

### 4.3.6.Atomic Force microscopy(AFM) analysis

AFM allows surface imaging of the sample in three-dimensional area. Further, it was analyzed by AFM (NT-MDT model, NTEGRA, Russia). The samples were prepared as a thin coating in a glass slide and allowed to completely air dried. The dried sample was analyzed for its peak height, size, skewness and kurtosis distribution data according to the ragothaman M et al[32].

### 4.3.7. High Resolution Transmission microscopy (HR-TEM) and Energy Dispersive X-ray Spectroscopy (EDS)

To assess the size and morphology of Col-AgNP-MUP was studied using HR-TEM (JEOL JEM 2100, Japan). The appropriate amount of sample was placed in grid and precoated with 1% (w/v) phosphotungstic acid for negative staining and allowed it for rapid drying. Lanthanum hexaboride is used as an electron source with the accelerated voltage of 200 kV and Selected Area Electron Diffraction (SAED) pattern are also studied. The elemental composition was determined by EDS (SIGMA HV – Carl Zeiss with Bruker Quantax. 200 – Z10 EDS Detector) [40].

### 4.3.8. In-vitro release and kinetic mechanism assessment

In brief, the dialysis bag method was used to study the *in-vitro* drug release. The drug release profile of the optimized formulation was analyzed in phosphate buffer saline (PBS) with varying pH values (pH 5.5, 6.8, 7.4) at 37 °C. Each sample that contained 1 mg/ml of 2 ml sample was transferred inside the dialysis bag (donor compartment) and it was placed in a beaker having 200 ml (receptor compartment) of buffer solution. The medium was stirred continuously using a magnetic stirrer (REMI, Maharashtra) set to 100 rpm. Followed by 4 ml of sample was periodically withdrawn and replaced at various timings. The released amount of drug in percentage was measured as mean ± SD at 222 nm by UV-visible spectrophotometer. The release kinetic was calculated using a DD solver. Regression coefficient ($R^2$) value analysis was used to identify the accurate fit with a kinetic model to the release data[40].

### 4.3.9. In-vitro cytotoxicity study

The cytotoxicity assay was carried out in the 3T3-L1 cell line using MTT (3-[4, 5-dimethylthiazol-2-yl]-2,5 diphenyl tetrazolium bromide)for the optimized formulation. In brief 3T3- L1 cells were seeded in 96 well plates with a density of $1×10^4$ cells/ml with Dulbecco modified Eagle's medium (Himedia, India) and allowed to grow for 2 days under 5% $CO_2$ at 37° C by renewing culture media every day to facilitate initial cell attachment. The sample, Col-AgNP-MUP was treated and incubated for 24 hr. Followed by, 10 µl of MTT (5mg/ml) solution was added to every well and incubated for 4 hrs. After 4 hrs, each well received 100 µl of DMSO to dissolve the formed formazan crystals. Finally, the absorbance was read at 570 nm using an ELISA reader[41].

### 4.4. Stability assessment

Based on the International Conference on Harmonization (ICH, Q1A) recommendations, the stability study was carried out. The stability of the optimized formulation samples was stored over 6 months at three different storage temperatures termed 04 ± 0.5 °C/no RH(relative humidity), 25 ± 0.2 °C/60 ± 5%, and 30 ± 2

°C/65 ± 5 %. The variations in PS, ZP, PDI, EE, and colour were assessed at the predefined time periods of 0, 1, 3, and 6 months[50].

## 4.5. Statistical analysis

All the experiment data represented as the mean ±SD, using statistics. The statistics analysis was performed using Design-Expert 13, graph pad prism 8 and origin-pro 2021 software. The variables were compared using a One- way ANOVA and $p < 0.05$ was referred as minimum significance.

**Author contributions:** Concept – V.S., M.R., B.R.; Design – V.S., M.R., B.R.; Supervision – V.S., M.R.; Resources – V.S., M.R., B.R.; Materials – V.S., M.R., B.R.; Data Collection and/or Processing – B.R.; Analysis and/or Interpretation – V.S., M.R., B.R.; Literature Search – B.R.; Writing – V.S., M.R., B.R.; Critical Reviews – V.S.,M.R., B.R.;

**Conflict of interest statement:** The authors declared no conflict of interest in the manuscript.

## REFERENCES

[1] Kular JK, Basu S, Sharma RI. The extracellular matrix: Structure, composition, age-related differences, tools for analysis and applications for tissue engineering. Tissue Eng. 2014;5:2041731414557112. https://doi.org/10.1177/2041731414557112.

[2] Martinengo L, Olsson M, Bajpai R, Soljak M, Upton Z, Schmidtchen A, Car J, Järbrink K. Prevalence of chronic wounds in the general population: systematic review and meta-analysis of observational studies. Ann Epidemiol. 2019; 29(1): 8-15. https://doi.org/10.1016/j.annepidem.2018.10.005.

[3] Monika P, Chandraprabha MN, Rangarajan A, Waiker PV, Chidambara Murthy KN. Challenges in healing wound: Role of complementary and alternative medicine. Front Nutr. 2022; 20(8):791-899. https://doi.org/10.3389/fnut.2021.791899.

[4] Olsson M, Järbrink K, Divakar U, Bajpai R, Upton Z, Schmidtchen A, Car J. The humanistic and economic burden of chronic wounds: A systematic review. Wound Repair Regen. 2019; 27(1):114-125. https://doi.org/10.1111/wrr.12683.

[5] Malta MD, Cerqueira MT, Marques AP. Extracellular matrix in skin diseases: The road to new therapies.J Adv Res. 2023; 51(9):149-160. https://doi.org/10.1016/j.jare.2022.11.008.

[6] Muthukumar T, Sreekumar G, Sastry TP, Chamundeeswari M. Collagen as a potential biomaterial in biomedical applications. Rev Adv Mater Sci. 2018;53(1):29-39.https://doi.org/10.1515/rams-2018-0002.

[7] Lin K, Zhang D, Macedo MH, Cui W, Sarmento B, Shen G. Advanced collagen-based biomaterials for regenerative biomedicine. Adv Funct Mater.2019; 29(3):1804-1943**.** https://doi.org/10.1002/adfm.201804943.

[8] Lamb YJ. Overview of the role of mupirocin. J Hosp Infect. 1991;19(9): 27-30. https://doi.org/10.1016/0195-6701(91)90199-i.

[9] Golmohammadi R, Najar-Peerayeh S, Tohidi Moghadam T, Hosseini SMJ. Synergistic antibacterial activity and wound healing properties of selenium-chitosan-mupirocin nanohybrid system: An in vivo study on rat diabetic *Staphylococcus aureus* wound infection model. Sci Rep. 2020;10(1): 2854. https://doi.org/10.1038/s41598-020-59510-5.

[10] Barroso A, Mestre H, Ascenso A, Simões S, Reis C. Nanomaterials in wound healing: From material sciences to wound healing applications. Nano Select. 2020;1(5):443-460. https://doi.org/10.1002/nano.202000055.

[11] Gunasekaran T, Nigusse T, Dhanaraju MD. Silver nanoparticles as real topical bullets for wound healing. J Am Coll Wound Spec.2012;3(4):82-96.https://doi.org/10.1016/j.jcws.2012.05.001.

[12] Dahmash EZ, Al-Khattawi A, Iyire A, Al-Yami H, Dennison TJ, Mohammed AR. Quality by Design (QbD) based process optimisation to develop functionalised particles with modified release properties using novel dry particle coating technique. PLoS One. 2018;13(11): e0206651. https://doi.org/10.1371/journal.pone.0206651.

[13] Cardoso VS, Quelemes PV, Amorin A, Primo FL, Gobo GG, Tedesco AC, Mafud AC, Mascarenhas YP, Corrêa JR, Kuckelhaus SA, Eiras C, Leite JR, Silva D, dos Santos Júnior JR. Collagen-based silver nanoparticles for biological applications: synthesis and characterization. J Nanobiotechnology. 2014; 12(9):36 https://doi.org/10.1186/s12951-014-0036-6.

[14] Chouhan P, Saini TR. Hydroxypropyl- β -cyclodextrin: A novel transungual permeation enhancer for development of topical drug delivery system for onychomycosis. J Drug Deliv. 2014; 2014:950358. https://doi.org/10.1155/2014/950358.

[15] Koilpillai J, Narayanasamy D. Development and characterization of novel surface engineered Depofoam: a QbD coupled failure modes and effects analysis risk assessment -based optimization studies. J Liposome Res. 2023; 5(5):1-17. https://doi.org/10.1080/08982104.2023.2208662.

[16] Uciński D. D-optimal sensor selection in the presence of correlated measurement noise. Measurement. 2020; 164:107873. https://doi.org/10.1016/j.measurement.2020.107873

[17] Chauhan B, Gupta R. Application of statistical experimental design for optimization of alkaline protease production from *Bacillus* sp. RGR-14. Process Biochem.2004;39(12):2115-2122. https://doi.org/10.1016/j.procbio.2003.11.002.

[18] Craciunescu O, Seciu AM, Manoiu VS, Trif M, Moisei M, Nicu AI, Zarnescu O. Biosynthesis of silver nanoparticles in collagen gel improves their medical use in periodontitis treatment. Part Sci Technol. 2018;37(6):757-763. .https://doi.org/10.1080/02726351.2018.1455780.

[19] Alam A, Foudah AI, Alqarni MH, Yusufoglu HS. Microwave-assisted and chemically tailored chlorogenic acid-functionalized silver nanoparticles of *Citrus sinensis* in gel matrix aiding QbD design for the treatment of acne. J Cosmet Dermatol. 2023; 22(5):1613-1627. https://doi.org/10.1111/jocd.15611.

[20] Reddy SG, Thakur A. Drug entrapment efficiency of silver nanocomposite hydrogel. InIOP Conference Series: Mater Sci Eng. 2019; 577 (1). https://doi.org/10.1088/1757-899X/577/12176.

[21] Jose RA, Merin DD, Arulananth TS, Shaik N. Characterization analysis of silver nanoparticles synthesized from chaetoceroscalcitrans. J Nanomater 2022;2022: 4056551. https://doi.org/1-15. 10.1155/2022/4056551.

[22] Begum R, Farooqi ZH, Naseem K, Ali F, Batool M, Xiao J, Irfan A. Applications of UV/Vis spectroscopy in characterization and catalytic activity of noble metal nanoparticles fabricated in responsive polymer microgels: A review. Crit Rev Anal Chem. 2018: 48(6):503-516. https://doi.org/10.1080/10408347.2018.1451299.

[23] Santhanam A, Sekar V, Kavitha NS. Facile synthesis and characterization of eco-friendly collagen based silver nanoparticles and its biological activities. Int J Res Appl Sci Eng Technol, 2023: 11(4): 4214-4223. https://doi.org/10.22214/ijraset.2023.51252 .

[24] Subha V, Kirubanandan S, Ilangovan R, Renganathan S. Silver nanoparticles impregnated nanocollagen as scaffold for soft tissue repair-synthesis, characterization, and ın-vitro ınvestigation. Int J Med Nano Res. 2021; 8:034. https://doi.org/23937/2378-3664.1410034.

[25] Lakkad HA, Patel VP. Design development and characterisation of mupirocin loaded emulsion based gel. Int J Pharm Sci Drug Res. 2021; 13(5): 543-552.https://doi.org/10.25004/ijpsdr.2021.130512.

[26] Ong TY, Shaik MI, Sarbon NM. Isolation and characterization of acid and pepsin soluble collagen extracted from sharpnose stingray (Dasyatiszugei) skin. Food Res. 2021;5(3):214-224.https://doi.org/10.22656/fr.2017.5(3).322.

[27] Ghanizadeh Gerayeli F, Hosseini F, Bagheri Z, Savardashtaki A, Shabaninejad Z, Amani AM, Najafipour S. Colorimetric sensor based on β-cyclodextrin-functionalized silver nanoparticles for zidovudine sensitive determination. Int J Anal Chem. 2020; 2020:5054864. https://doi.org/10.1155/2020/5054864.

[28] Budhiraja M, Zafar S, Akhter S, Alrobaian M, Rashid MA, Barkat MA, Beg S, Ahmad FJ. Mupirocin-loaded chitosan microspheres embedded in *Piper betle* extract containing collagen scaffold accelerate wound healing activity. AAPS PharmSciTech. 2022: 23(3): 77.https://doi.org/10.1208/s12249-022-02233-9.

[29] Verma J, Kanoujia J, Parashar P, Tripathi CB, Saraf SA. Wound healing applications of sericin/chitosan-capped silver nanoparticles incorporated hydrogel. Drug DelivTransl Res. 2017; 7(1):77-88. https://doi.org/10.1007/s13346-016-0322-y.

[30] Yerragopu PS, Hiregoudar S, Nidoni U, Ramappa KT, Sreenivas AG, Doddagoudar SR. Chemical synthesis of silver nanoparticles using tri-sodium citrate, stability study and their characterization. Int Res J Pure Appl Chem, 2020: 21(3):37-50. https://doi.org/10.9734.IRJPAC/2020/v21i330159.

[31] Htwe YZ, Chow WS, Suda Y, Mariatti M. Effect of silver nitrate concentration on the production of silver nanoparticles by green method. Mater Today. 2019; 17(1):568-573. https://doi.org/10.1016/j.matpr.2019.06.336.

[32] Ragothaman M, Kannan Villalan A, Dhanasekaran A, Palanisamy T. Bio-hybrid hydrogel comprising collagen-capped silver nanoparticles and melatonin for accelerated tissue regeneration in skin defects. Mater Sci Eng C Mater Biol Appl. 2021; 128(9):112328. https://doi.org/10.1016/j.msec.2021.112328.

[33] Kotakadi VS, Gaddam SA, Venkata SK, Sarma PV, Sai Gopal DV. Biofabrication and spectral characterization of silver nanoparticles and their cytotoxic studies on human CD34 +ve stem cells. 3 Biotech. 2016; 6(2): 216. https://doi.org/10.1007/s13205-016-0532-5.

[34] Morones JR, Elechiguerra JL, Camacho A, Holt K, Kouri JB, Ramírez JT, Yacaman MJ. The bactericidal effect of silver nanoparticles. Nanotechnology. 2005;16(10):2346-2353.https://doi.org/10.1088/0957-4484/16/10/059.

[35] Khane Y, Benouis K, Albukhaty S, Sulaiman GM, Abomughaid MM, Al Ali A, Aouf D, Fenniche F, Khane S, Chaibi W, Henni A, Bouras HD, Dizge N. green synthesis of silver nanoparticles using aqueous *Citrus limon* zest extract: Characterization and evaluation of their antioxidant and antimicrobial properties. Nanomater. 2022;12(12):2013. https://doi.org/10.3390/nano12122013.

[36] Miranda-Calderon L, Yus C, Landa G, Mendoza G, Arruebo M, Irusta S. Pharmacokinetic control on the release of antimicrobial drugs from pH-responsive electrospun wound dressings.Int J Pharm. 2022; 624(8): 122003.https://doi.org/10.1016/j.ijpharm.2022.122003.

[37] Paarakh MP, Jose PA, Setty CM, Peterchristoper GV. Release kinetics–concepts and applications. Int J PharmTechnol. 2018;8(1):12-20.https://doi.org/10.31838/ijprt/08.01.02.

[38] Sritharadol R, Nakpheng T, Wan Sia Heng P, Srichana T. Development of a topical mupirocin spray for antibacterial and wound-healing applications. Drug Dev Ind Pharm. 2017;43(10):1715-1728. https://doi.org/10.1080/03639045.2017.1339077.

[39] Ahmad N, Fozia, Jabeen M, Haq ZU, Ahmad I, Wahab A, Islam ZU, Ullah R, Bari A, Abdel-Daim MM, El-Demerdash FM, Khan MY. Green fabrication of silver nanoparticles using *Euphorbia serpens* Kunth aqueous extract, their characterization, and investigation of its *in vitro* antioxidative, antimicrobial, insecticidal, and cytotoxic activities. Biomed Res Int. 2022. https://doi.org/10.1155/2022/5562849.

[40] Tavares Luiz M, Santos Rosa Viegas J, Palma Abriata J, Viegas F, Testa Moura de Carvalho Vicentini F, Lopes Badra Bentley MV, Chorilli M, Maldonado Marchetti J, Tapia-Blácido DR. Design of experiments (DoE) to develop and to optimize nanoparticles as drug delivery systems.Eur J Pharm Biopharm. 2021;165(5):127-148. https://doi.org/10.1016/j.ejpb.2021.05.011.

[41] Najm MB, Rawas-Qalaji M, Assar NH, Yahia R, Hosary RE, Ahmed IS. Optimization, characterization and in vivo evaluation of mupirocin nanocrystals for topical administration. Eur J Pharm Sci. 2022;176(9):106251. https://doi.org/ 10.1016/j.ejps.2022.106251.

[42] Priyanka S, Nithya R. lisinopril dihydrate loaded nano-spanlastic bio-adhesive gel for intranasal delivery: 2³ factorial optimization, fabrication and ex-vivo studies for enhanced mucosal permeation. J Pharm Res. 2022;26(4):884-899. https://dx.doi.org/10.29228/jrp.187.

[43] Rajan durai B.R, Sankar V, Koilpillai J. Isolation and characterization of collagen from tannery waste for biomedical applications. BioNanoSci. 2023; 13( 4): 2033-2048. https://doi.org/10.1007/s12668-023-01228-5.

[44] Andrade PF, de Faria AF, da Silva DS, Bonacin JA, Gonçalves Mdo C. Structural and morphological investigations of β-cyclodextrin-coated silver nanoparticles. Colloids Surf B Biointerfaces. 2014;118(6): 289-297. https://doi.org/10.1016/j.colsurfb.2014.03.032.

[45] Hwang J, Huang H, Sullivan MO, Kiick KL. Controlled delivery of vancomycin from collagen-tethered peptide vehicles for the treatment of wound ınfections. Mol Pharm. 2023; 20(3):1696-1708. https://doi.org/10.1021/acs.molpharmaceut.2c00898.

[46] Varela-Fernández R, García-Otero X, Díaz-Tomé V, Regueiro U, López-López M, González-Barcia M, Isabel Lema M, Javier Otero-Espinar F. Lactoferrin-loaded nanostructured lipid carriers (NLCs) as a new formulation for optimized ocular drug delivery. Eur J Pharm Biopharm. 2022; 172(3):144-156. https://doi.org/10.1016/j.ejpb.2022.02.010.

[47] Srivatsan KV, Duraipandy N, Begum S, Lakra R, Ramamurthy U, Korrapati PS, Kiran MS. Effect of curcumin caged silver nanoparticle on collagen stabilization for biomedical applications. Int J Biol Macromol. 2015;75(1):306-315. https://doi.org/10.1016/j.ijbiomac.2015.01.050.

[48] Sahoo D, Singh VK, Agrahari K, Kumari KU, Luqman S, Savita A, Gupta H, Rout PK, Yadav NP. Development of QbD-based mupirocin-β-cyclodextrin complex loaded thermosensitivein-situgel for wound healing in mice. J Drug Deliv Sci Technol. 2023;19(5):104585.https://doi.org/10.1016/j.dddst.2023.104585.

[49] Rahman SM, Sharma P, Said Z. Application of response surface methodology based D-optimal design for modeling and optimisation of osmotic dehydration of zucchini. Chem Eng J. 2022;4(9):100039.https://doi.org/10.1016/j.dche.2022.100039.

[50] Badhwar R, Singh R, Popli H. Implementation of quality by design (qbd) approach in development of qct-smedds with combination of agnps for diabetic foot ulcer management. Indian J Pharm Educ Res. 2021; 55(4):1207-1223.https://doi.org/10.1016/ijbiomac.2015.010050.